

# Chemiluminescence Measurements and Modeling in Syngas, Methane and Jet-A Fueled Combustors

Venkata N. Nori\* and Jerry M. Seitzman†

*Guggenheim School of Aerospace Engineering*

*Georgia Institute of Technology*

*Atlanta, GA, USA 30332-0150*

The chemiluminescence from  $\text{CO}_2^*$ ,  $\text{OH}^*$  and  $\text{CH}^*$  are investigated using state-of-the-art mechanisms and rate models for excited state formation and quenching applied to detailed chemical kinetic models for gaseous and liquid fuels used in gas turbine systems. The models are first validated by comparison to experimental data acquired in lean premixed flames. The experimental chemiluminescence spectra were obtained in laminar Bunsen flames for  $\text{CO}/\text{H}_2$  (syngas) fuel mixtures and in a swirl-stabilized combustor for methane. Emission from the  $\text{OH } A^2\Sigma$  state at  $309\pm 5\text{nm}$ , the  $\text{CO}_2$  continuum at  $375\pm 1\text{nm}$  and the  $\text{CH } A^2\Delta$  state at  $430\pm 5\text{nm}$  are extracted from the spectra. Comparisons are presented for the ratio of chemiluminescence signals and for the individual signals over a range of equivalence ratios ( $\phi$ ) and, for the syngas fuels, with reactant preheating and dilution. The model results for all three species are in good agreement with the experiments, except in the swirl-stabilized combustor near its lean blowout limit, where the assumptions embedded in the ideal 1-d, adiabatic flame model used are likely to fail. The models are then used to analyze chemiluminescence for equivalence ratio and heat release rate sensing in methane and Jet-A fuel combustion. The ratio of  $\text{CH}^*$  to  $\text{OH}^*$  emission is found to be a good indicator of equivalence ratio for methane flames, increasing monotonically from  $\phi\sim 0.7$  to at least 1.3; for Jet-A flames, however, the model shows the ratio is non-monotonic, with a minimum near  $\phi=0.75$ . For all the fuels studied, all three chemiluminescence sources are less than ideal indicators of heat release if the equivalence ratio of the flame is also changing significantly, since the emission intensity normalized by the fuel consumption rate is dependent on  $\phi$ . For syngas and methane systems,  $\text{CO}_2^*$  chemiluminescence shows the least variation. For Jet-A, all three species have similar variations; the best choice for minimizing  $\phi$  effects depends on the  $\phi$  and temperature range of interest.

## I. Introduction

Flame chemiluminescence has received renewed attention for combustion sensing and diagnostic applications due to its simplicity and non-intrusive nature. The radiative emission from electronically excited species such as  $\text{CH}^*$ ,  $\text{OH}^*$ ,  $\text{C}_2^*$  and  $\text{CO}_2^*$  are the primary sources of chemiluminescence in typical hydrocarbon-air flames.<sup>1</sup> Chemiluminescence from a species can provide information on the concentration of its precursors, and can be indicative of important combustion parameters that relate to combustor performance, pollutant formation and combustor health. Systematic investigations of the ratios of emissions from excited species show promise for an equivalence ratio sensor in both gaseous and liquid systems.<sup>2-5</sup> Chemiluminescence imaging of excited radicals has found considerable application in reaction zone marking.<sup>6</sup> Chemiluminescence has been used to characterize temporal fluctuations in the overall heat release and the spatial distribution of the local heat release in applications

\* Graduate Research Assistant (AIAA Student Member)

† Associate Professor (AIAA Associate Fellow)

related to combustion instabilities.<sup>7,8</sup> However, care must be taken to interpret these line of sight global measurements.<sup>9</sup>

While there have been numerous experimental investigations and applications of chemiluminescence in flames, there have been few modeling efforts. The ability to model and predict chemiluminescence would help in gaining better understanding of the chemiluminescence processes and the dependence of chemiluminescence signals on vital combustion parameters. It would also be of great help in developing combustion diagnostics/sensors and interpreting the resulting data. Addition of kinetic rate expressions for excited-state species to detailed chemical kinetic models has been used to estimate chemiluminescence rate constants (in a low pressure flame)<sup>10</sup> and to understand the relationships between chemiluminescence and flame properties.<sup>12</sup> These studies examined OH\*, CH\* and C<sub>2</sub>\* in premixed methane systems; CO<sub>2</sub>\* chemiluminescence was not considered. Numerical investigation of CO<sub>2</sub>\* chemiluminescence and its relevance in laminar and turbulent premixed flames was evaluated by Samaniego *et al.*<sup>13</sup>, but there was no experimental validation.

The goal of the current study is to examine OH\*, CO<sub>2</sub>\* and CH\* chemiluminescence in various fuel-air systems. OH\*, CH\* and CO<sub>2</sub>\* chemiluminescence were chosen as they occur in almost all hydrocarbon flames, including lean systems relevant to low NO<sub>x</sub> emissions. Moreover, there is an extensive body of work on the reactions and rate constants for the formation and destruction of these excited species, especially with regard to OH\* and CO<sub>2</sub>\*. First, experimental data is acquired at various operating conditions in order to evaluate the chemiluminescence models. Two types of fuels were chosen for this evaluation: methane and mixtures of H<sub>2</sub> and CO. These fuels were chosen since there are well-validated, detailed mechanisms for combustion of these fuels. In addition, these fuels are highly relevant to many stationary combustion systems, such as gas turbines. Methane is the primary ingredient in natural gas, and H<sub>2</sub>/CO are the primary constituents in synthetic gas (or syngas), along with CH<sub>4</sub> and diluents such as N<sub>2</sub>, CO<sub>2</sub> and H<sub>2</sub>O.<sup>14</sup> In the second half of this study, the validated models are applied to both the gaseous fuels and Jet-A, with the latter chosen for its relevance to aircraft propulsion applications. The goal is to determine the ability of flame chemiluminescence to be used for sensing important combustion parameters, such as heat release rate and reaction zone equivalence ratio.

## II. Background

Emission from the electronically excited OH A<sup>2</sup>Σ<sup>+</sup> state (typically denoted OH\* in the flame chemiluminescence literature) near 310 nm is a prominent feature of hydrogen and hydrocarbon flame spectra. OH\* emission and the reactions responsible for the formation of OH\* have long been studied,<sup>15-18</sup> starting from the early work of Gaydon to the most recent work in shock tubes by Petersen *et al.*<sup>19</sup> Proposed reaction mechanisms consist of the following general steps: 1) excited state formation reactions, 2) (rapid) collisional quenching reactions that remove the excited state, reducing OH to its ground electronic configuration, and 3) radiative transitions to the OH ground state. Among these steps the formation reactions are the ones that are most difficult to determine. Most investigations have pointed to the following reactions as the key formation steps:



R1 and R2 are typically presented as the main formation reactions in hydrogen flames, while R3 is used for hydrocarbon flames. In this study, a model based on R1 only was used for the syngas flames, and both R1 and R3 for hydrocarbon flames (e.g., methane and Jet-A). The complete OH\* mechanism with the reactions and their associated rate parameters are given in Table 1. In flames, electronically excited species in general have low concentrations due to their low production rates and their rapid removal by collisional quenching. They therefore often have little impact on the overall flame chemistry. For these reasons, OH\* can often be assumed to be in quasi-steady state, with the formation rate limiting the whole process.<sup>20</sup> Under these conditions, the concentration of OH\* (e.g., moles/cm<sup>3</sup>) is given by

$$[\text{OH}^*] = \frac{k_1[\text{O}][\text{H}][\text{M}] + k_3[\text{CH}][\text{O}_2]}{\sum_j k_j[\text{M}_j] + A} \quad (1)$$

where  $k_1$  and  $k_3$  are the rate constants of the formation reactions,  $k_j$  is the quenching rate constant for  $\text{OH}^*$  by species  $j$  and  $A$  is the Einstein coefficient for spontaneous emission for the  $A \rightarrow X$  transition. The photon emission rate  $i$  (mole photons/cm<sup>3</sup>/sec) for the chemiluminescence can then be found via the simple relation

$$i_{\text{OH}^*} = A_{kl}[\text{OH}^*] \quad (2)$$

where  $A_{kl}$  is the effective band  $A$  coefficient for the vibrational bands included in the detection bandwidth.

Table 1. Chemiluminescence reaction mechanisms used to model  $\text{OH}^*$  and  $\text{CH}^*$  formation and quenching. The Einstein  $A$  coefficients for  $\text{CH}^*$  and  $\text{OH}^*$  are  $1.85 \times 10^6 \text{ s}^{-1}$  [Ref. 21] and  $1.4 \times 10^6 \text{ s}^{-1}$  [Ref. 18].

	Reaction	A	B	E <sub>a</sub>	Ref.
R1	$\text{H} + \text{O} + \text{M} \leftrightarrow \text{OH}^* + \text{M}$	$6 \times 10^{14}$	0.0	6940	19
R3	$\text{CH} + \text{O}_2 \leftrightarrow \text{OH}^* + \text{CO}$	$3.24 \times 10^{14}$	-0.4	4150	22
Q1 <sub>OH</sub>	$\text{OH}^* + \text{H}_2\text{O} \rightarrow \text{OH} + \text{H}_2\text{O}$	$5.92 \times 10^{12}$	0.5	-861	22
Q2 <sub>OH</sub>	$\text{OH}^* + \text{CO}_2 \rightarrow \text{OH} + \text{CO}_2$	$2.75 \times 10^{12}$	0.5	-968	22
Q3 <sub>OH</sub>	$\text{OH}^* + \text{CO} \rightarrow \text{OH} + \text{CO}$	$3.23 \times 10^{12}$	0.5	-787	22
Q4 <sub>OH</sub>	$\text{OH}^* + \text{H}_2 \rightarrow \text{OH} + \text{H}_2$	$2.95 \times 10^{12}$	0.5	-444	22
Q5 <sub>OH</sub>	$\text{OH}^* + \text{O}_2 \rightarrow \text{OH} + \text{O}_2$	$2.10 \times 10^{12}$	0.5	-482	22
Q6 <sub>OH</sub>	$\text{OH}^* + \text{OH} \rightarrow \text{OH} + \text{OH}$	$1.50 \times 10^{12}$	0.5	0.0	22
Q7 <sub>OH</sub>	$\text{OH}^* + \text{H} \rightarrow \text{OH} + \text{H}$	$1.50 \times 10^{12}$	0.5	0.0	18
Q8 <sub>OH</sub>	$\text{OH}^* + \text{O} \rightarrow \text{OH} + \text{O}$	$1.50 \times 10^{12}$	0.5	0.0	18
Q9 <sub>OH</sub>	$\text{OH}^* + \text{N}_2 \rightarrow \text{OH} + \text{N}_2$	$1.08 \times 10^{11}$	0.5	-1238	18
Q10 <sub>OH</sub>	$\text{OH}^* + \text{CH}_4 \rightarrow \text{OH} + \text{CH}_4$	$3.36 \times 10^{12}$	0.5	-635	18
R6	$\text{C}_2\text{H} + \text{O} \leftrightarrow \text{CH}^* + \text{CO}$	$6.023 \times 10^{12}$	0.0	457	20
R7	$\text{C}_2\text{H} + \text{O}_2 \leftrightarrow \text{CH}^* + \text{CO}_2$	$6.023 \times 10^{-4}$	4.4	-2285.1	20
Q1 <sub>CH</sub>	$\text{CH}^* + \text{H}_2\text{O} \leftrightarrow \text{CH} + \text{H}_2\text{O}$	$5.3 \times 10^{13}$	0.0	0.0	21
Q2 <sub>CH</sub>	$\text{CH}^* + \text{CO}_2 \leftrightarrow \text{CH} + \text{CO}_2$	$2.41 \times 10^{-1}$	4.3	-1694	21
Q3 <sub>CH</sub>	$\text{CH}^* + \text{CO} \leftrightarrow \text{CH} + \text{CO}$	$2.44 \times 10^{12}$	0.5	0.0	21
Q4 <sub>CH</sub>	$\text{CH}^* + \text{H}_2 \leftrightarrow \text{CH} + \text{H}_2$	$1.47 \times 10^{14}$	0.0	1361	21
Q5 <sub>CH</sub>	$\text{CH}^* + \text{O}_2 \leftrightarrow \text{CH} + \text{O}_2$	$2.48 \times 10^6$	2.14	-1720	21
Q6 <sub>CH</sub>	$\text{CH}^* + \text{N}_2 \leftrightarrow \text{CH} + \text{N}_2$	$3.03 \times 10^2$	3.4	-381	21
Q7 <sub>CH</sub>	$\text{CH}^* + \text{CH}_4 \rightarrow \text{CH} + \text{CH}_4$	$1.73 \times 10^{13}$	0.0	167	21

Rate coefficients are expressed as  $K = A T^n \exp(-E/RT)$  with units of cal, mol, cm and s.

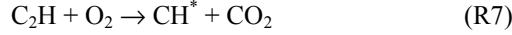
The origin and the structure of the  $\text{CO}_2^*$  “blue continuum” have also been investigated by various groups. In a series of experiments, Pravilov *et al.*<sup>23</sup> identified the formation reactions responsible for producing excited state  $\text{CO}_2^*$ , which can then radiatively and non-radiatively transition to the ground state. The  $\text{CO}_2^*$  continuum has a spectral shape that changes only slightly over a range of conditions. The global  $\text{CO}_2^*$  formation reaction based on the work of Pravilov *et al.* is



Therefore, the photon emissions rate  $i_{\text{CO}_2^*}$  is found to be dependent on the concentrations of  $[\text{CO}]$  and  $[\text{O}]$ .<sup>24</sup> The rate expression for the emission due to the chemiluminescence reaction in the temperature range 1300-2700 K was found at 375 nm from the spectral data reported by Slack *et al.*<sup>25</sup> and is given by

$$i_{\text{CO}_2^*} = 3.3(\pm 0.3) \times 10^3 \exp[-2300/T(K)][\text{CO}][\text{O}] \quad (3)$$

The characteristic blue chemiluminescence observed in hydrocarbon flames around 430 nm is due to CH\* emission, specifically the (0, 0) band of the CH (A<sup>2</sup>Δ - X<sup>2</sup>Π) transition. There is still debate on the important formation reactions responsible for CH\*. Of the many plausible sources, research has focused on the following.



Gaydon<sup>26</sup> suggested the reaction R5; this was later challenged, first by Brenig<sup>27</sup> and later by Grebe and Homann.<sup>28</sup> Brenig's experiments suggested that the CH\* radical might be produced from the reaction of ground state ethynyl radicals with O atoms, which had been earlier proposed by Glass *et al.*<sup>29</sup> Renlund *et al.*<sup>30</sup> suggested the reaction (R7) of C<sub>2</sub>H with O<sub>2</sub> rather than atomic oxygen. Devriendt *et al.*<sup>31</sup> in their pulse laser photolysis study at low pressure determined the temperature dependence of R6 and concluded that the majority of CH\* is produced by that reaction. However in a recent study by Carl *et al.* based on flash photolysis of acetylene at low pressure<sup>32</sup>, the temperature dependence of R7 was found; they also suggested that R7 might contribute significantly to CH\* chemiluminescence in hot flames and especially under fuel lean conditions. So, in this study, a model based on R6 and R7 was used to model CH\* in methane and Jet-A flames. The complete CH\* mechanism with the reactions and their associated rate parameters are given in Table 1. As in the OH\* analysis, the photon emission rate  $i_{\text{CH}^*}$  is found from the quasi-steady concentration [CH\*] using CH\* collisional quenching and spontaneous emission rates.

### III. Experimental Setup

#### A. Burners

Chemiluminescence spectra were acquired in two premixed burners: the syngas fuels used a laminar jet flame as shown in Figure 1a. This burner was previously used to measure laminar flame speeds for syngas mixtures, and its details including syngas mixture preparation can be found there.<sup>24</sup> The burner is a straight cylindrical stainless steel tube with an inner diameter of 4.5mm, the length of which is ensured to make the flow laminar and exit velocity profile fully developed. The rotameters used for flow rate measurements were calibrated with a bubble flow meter to ±1% accuracy, implying a maximum error of 4% in equivalence ratio. To study the effects of preheating, the reactants can be heated by electrical resistance tape wound around the burner tube. The data presented here correspond to mixtures with H<sub>2</sub>:CO volumetric ratios of 50:50 and 33:67. Additionally for the H<sub>2</sub>:CO =50:50 mixture, two further cases were studied: reactant preheating to ~500K and 20% dilution with CO<sub>2</sub>.

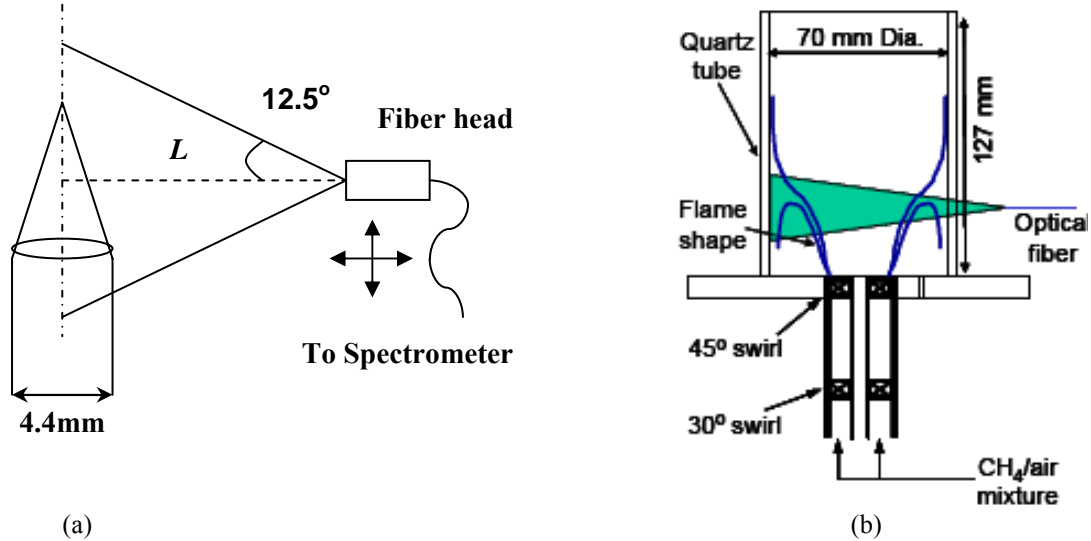


Figure 1. Burner schematics for (a) laminar jet flame for syngas measurements and (b) swirl combustor for methane studies.

The methane combustor configuration (Figure 1b) is a swirl stabilized combustor with a (theoretical) swirl number of 0.66 used in a previous chemiluminescence study.<sup>4</sup> The combustor is a dump type configuration with the cylindrical dump plane being 70mm in diameter and 127mm long. The quartz walls of the test section facilitate detection of ultraviolet (UV) flame emission. The data presented here correspond to a bulk average, (cold) velocity of 5 m/s in the test section.

## B. Detection Optics

The optical emission from these combustors was detected using a fiber-optic based collection system coupled to an imaging spectrometer. The fiber collection array consisted of four bundles, each bundle having three 200 $\mu$ m fused silica fibers with a numerical aperture of 0.22. The outlet end of the fibers were located at the entrance slit of a 300mm imaging spectrometer (Acton Spectra-Pro 300i, 300 grooves/mm grating), with a 16-bit, 1024 $\times$ 256 intensified CCD camera (PI-MAX, 25 mm intensifier) at the exit plane that was used to detect and record the flame emission spectrum. The grating dispersion allowed simultaneous capture of the ultraviolet and visible optical emission spectrum in the range of  $\sim$ 260–540 nm. The resolution of the spectrometer was  $\sim$ 2 nm with the entrance slit width set to 100  $\mu$ m. Diffusely scattered light from a 633nm He-Ne laser beam was used to experimentally determine the spectrometer resolution. In most cases, ten exposures were acquired at each operating conditions, with a camera exposure time of 100 ms. The ten exposures were averaged and background corrected before extracting the OH\* and CO<sub>2</sub>\* chemiluminescence. Typical flame spectra are shown in Figure 2.

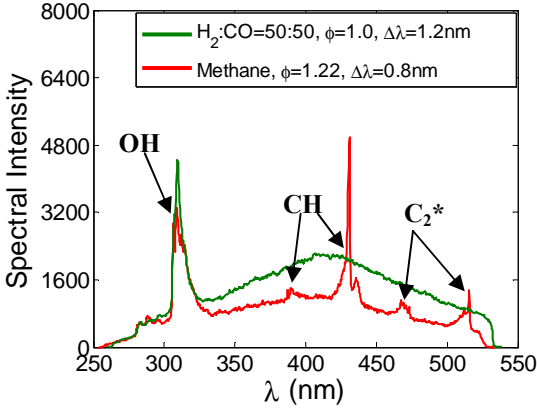


Figure 2. Typical flame spectra in syngas and methane fuels.

As seen in Figure 1, the combustors had different fiber collection configurations because of the inherent differences in their flow fields. For the turbulent swirl combustor used for the methane measurements, the fiber was placed at a fixed location about 2 cm away from the combustor wall and 3 cm from the base of the combustor. This allowed the fiber to collect light from most of the flame region. Due to the swirl-stabilization, the size of the flame did not change greatly with changes in fuel-air ratio. As the syngas cases employed a conical jet flame, the total flame chemiluminescence was most efficiently captured by moving the fiber along a line perpendicular to the flame axis. The distance from the flame to the fiber was chosen such that the entire flame cone was just within the collection solid angle of the fiber. The syngas flames were 7.5-25 mm high, so the fiber was placed 70-115 mm from the flame.

In order to compare the absolute chemiluminescence from each flame, it is necessary to account for the change in light collection due to the distance ( $L$ ) between the fiber and flame. Each point of the flame emits light in all directions, but only the light which is in the solid angle subtended by the fiber optic relative to that point contributes to the total signal collected by the spectrometer-camera system. The detection system signal for excited-state species  $c$  (i.e., OH\*, CH\* or CO<sub>2</sub>\*) is given by

$$S_c = A_{rxn} I_c \frac{\Omega}{4\pi} R_{\lambda c} \Delta t_E \quad (4)$$

where  $A_{rxn}$  is the reaction zone surface area,  $I_c$  (photons/cm<sup>2</sup>/sec) is the average chemiluminescence intensity integrated across the flame thickness ( $\ell_f$ ), i.e.,

$$I_c = \int_0^{\ell_f} i_c dx \quad (5)$$

$\Omega$  is the collection solid angle, which is approximately given by  $\pi D^2/4L^2$  where  $D$  is the diameter of the fiber core,  $R_{\lambda,c}$  (counts/photon) is the wavelength dependent responsivity of the overall fiber/camera/spectrometer system and  $\Delta t_E$  is the exposure time of the camera.

#### IV. Chemiluminescence Modeling

OH\*, CO<sub>2</sub>\* and CH\* chemiluminescence was modeled in the syngas-air and methane-air flames using detailed chemical kinetics calculations for 1D, adiabatic and zero-strain premix flames (CHEMKIN™ PREMIX<sup>33</sup>) incorporating the GRIMech 3.0<sup>34</sup> reaction mechanism. For Jet-A, we replaced GRIMech with a reduced mechanism developed for Jet-A that includes 167 reactions and 63 species.<sup>35</sup> Multi-component diffusion and thermal diffusion were included since these effects can be important, especially in fuels with even moderate levels of hydrogen.

The important chemiluminescence reactions used here for OH\* and CH\* and their respective rate parameters are given in Table 1. While it is possible to add these rates into the detailed mechanism, it was found that postprocessing of the Chemkin output (using the quasi-steady assumption approach described above) produced essentially the same results since the excited state populations are small compared to the ground state species included in the detailed mechanism. For example, the peak OH\* concentration for the syngas fuels was eight orders of magnitude lower than those of the other species involved in its reactions. Additionally, the reaction rates of the other relevant species are typically 2-4 orders of magnitude higher than the formation or quenching rates of OH\*. For CO<sub>2</sub>\* chemiluminescence, the single expression given by equation (3) is sufficient. The profiles through the 1-d flames were integrated (as per equation (5)) up to a distance of 1 cm (well beyond the end of the primary reaction zone) to give  $I_{OH^*}$ ,  $I_{CH^*}$  and  $I_{CO_2^*}$  for comparison to the experimental data.

#### V. Results and Discussion

Two sets of studies were performed. In the first study, the current chemiluminescence model, based on rate data available in the literature (without modification) was validated against experimental results acquired across a range of conditions, including gaseous fuels. The second study utilized the model to better understand the use of chemiluminescence for combustion sensing/diagnostic applications.

##### A. Validation

###### Syngas Fuels

In order to compare the experimental results to the model predictions, it is most convenient to examine the chemiluminescence ratios. By taking the ratio of two species from equation (4), the chemiluminescence ratio (for example for CO<sub>2</sub>\* versus OH\*) is given by the expression

$$\frac{S_{CO_2^*}}{S_{OH^*}} = \frac{I_{CO_2^*} R_{\lambda,CO_2^*}}{I_{OH^*} R_{\lambda,OH^*}} \quad (6)$$

It is evident that the chemiluminescence ratios are independent of the imaged flame size (or surface area or mass flow rates) and collection optics arrangement, and only differ from the computations due to the change in system responsivity at different wavelengths. Thus if the modeling is faithful, then the simulation results should differ from the experimental data only by a single multiplicative constant ( $C_1$ ) for a given species ratio.

The comparison for the syngas fuel is considered first. A best fit was obtained with a constant  $C_1=20.8$  for the CO<sub>2</sub>\* /OH\* ratio as shown in Figure 3a. The data shown in Figure 3 include two fuel compositions, with the hydrogen to carbon monoxide ratio changing by a factor of two, a case where the reactants were preheated to ~200 °C (990 °F), and a case where the fuel was diluted with 20% CO<sub>2</sub>. While the fuel composition does little to change the flame temperature for a given equivalence ratio, preheating and dilution do have an effect. Overall, the agreement between the model results and the experimental data is quite good. This is perhaps clearer by examining the

percentage relative error (Figure 3b). The modeling results are within  $\pm 7\%$  of the experimental ratios for all the data points except one. The relative error is defined as

$$\% \text{ Rel Error} = \left[ \frac{C_1 \times (\text{ratio})_C - (\text{ratio})_E}{(\text{ratio})_E} \right] \times 100 \quad (7)$$

where the subscripts C and E correspond to the computational simulation and experiment ratios.

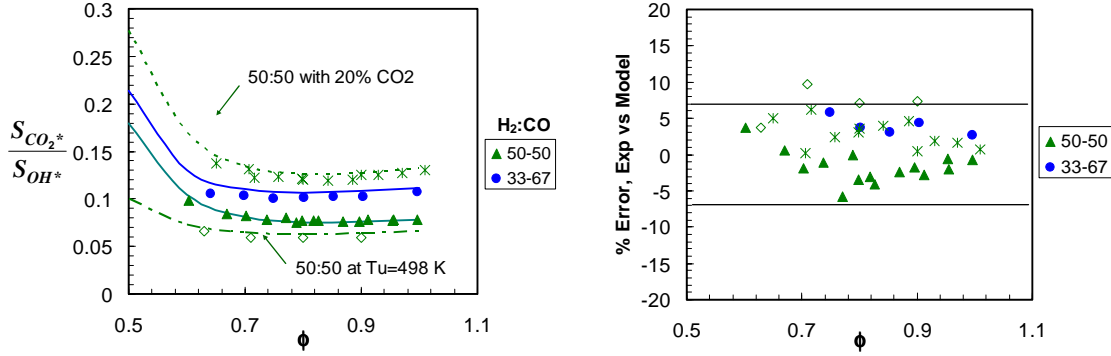


Figure 3. (a) Variation of  $CO_2^*$  to  $OH^*$  ratio in syngas fuel flames (data points are experiments, lines are modeling predictions) and (b) relative error between the experimental data and modeled ratios,  $\pm 7\%$  error levels are indicated by the horizontal lines.

It is possible for the ratios to match, even if there is an error in modeling the individual chemiluminescence signals, if the simulations for both signals contain the same errors. Therefore, we also examined the individual chemiluminescence signals for variations in the fuel-air ratio, fuel composition, preheat temperature and dilution. To compare the absolute signal for a given chemiluminescence species  $c$  ( $S_c$ ) with the 1-d simulations, equation (4) was modified as follows.

$$S_c = I_c \frac{\dot{m}}{\rho_u S_L} \frac{D^2}{16L^2} R_{\lambda c} \Delta t_E \quad (8)$$

In equation (8), the change in solid angle  $\Omega$  as the fiber was moved is modeled as a simple  $1/L^2$  variation, and the 1-d flame surface area was connected to the experimental mass flowrates using the 1-d flame speed expression, where  $\rho_u$  is the density of the unburned reactants and  $S_L$  is the flame speed determined from the simulations. Normalizing the measured signals by the fuel mass flow rates and combining all the variables that were held constant into the value  $C_c$ , we get a normalized chemiluminescence signal

$$\frac{S_c / \Delta t_E}{\dot{m}_f} = \frac{\dot{S}_c}{\dot{m}_f} = C_c \frac{\dot{m} / \dot{m}_f}{L^2 \rho_u S_L} I_c \quad (9)$$

where  $\dot{S}_c$  is the fluorescence signal rate, and the ratio of total mass flow rate to fuel mass flow rate is a function of reactant composition, e.g.,  $\phi$ . With equation (9), the simulations can be compared to the experimental results for total chemiluminescence signal.

The results are shown in Figure 4 for the  $OH^*$  normalized by the hydrogen fuel flow rate and  $CO_2^*$  normalized by the CO fuel flow rate. As with the ratio comparison, the ability of the model to simulate the measured flame emission signals is excellent for the baseline  $H_2:CO=50:50$  case. The agreement is also quite good in general for the preheated and  $CO_2$  diluted cases. As seen in the data, the models show the  $OH^*$  emission is more sensitive to preheating or dilution (and therefore possibly temperature) than the  $CO_2^*$  chemiluminescence. For the lower  $H_2$  content mixture ( $H_2:CO=33:67$ ), both the  $OH^*$  and  $CO_2^*$  signals are over predicted. This over prediction is similar in both cases, so the modeled chemiluminescence ratio (Figure 3) shows better agreement. The discrepancy may be due to errors in modeling the flame speed with the simple 1-d model and because flame speed is such a strong function of  $H_2$  content. Still the over predictions are not large, and it can be concluded that the syngas results provide ample verification that the the  $CO_2^*$  and  $OH^*$  models (at least for formation step (R1)) are accurate.

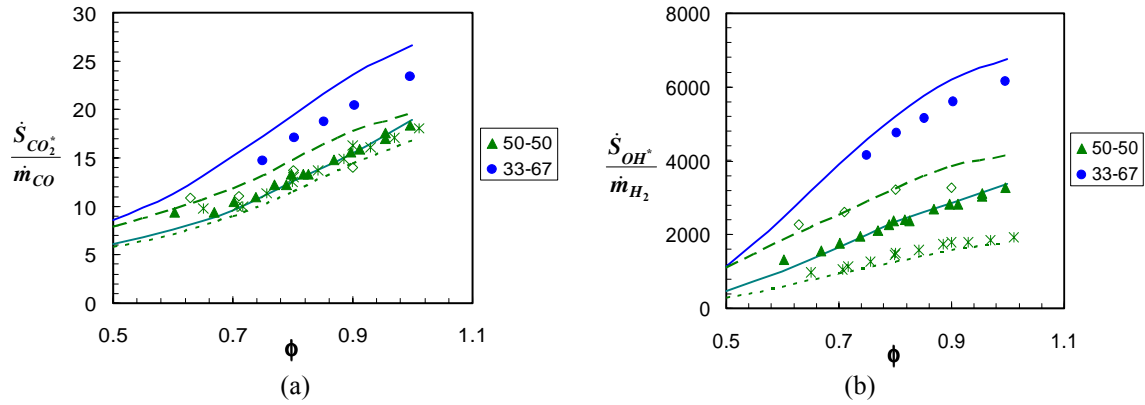


Figure 4. Comparison between measured and simulated integrated and normalized chemiluminescence for (a)  $CO_2^*$  emission and (b)  $OH^*$  for the syngas flames. The symbols represent the same conditions indicated in Figure 3.

### Methane

The validity of the model including the other  $OH^*$  formation reaction (R3) and the  $CH^*$  model can be tested by the use of a hydrocarbon fuel, methane in this case. As noted previously, the methane data were acquired in a more complex flowfield, a turbulent swirl combustor. Thus, these experiments are a further test of the validity of the models. As before, the chemiluminescence ratios are first compared between the experiments and modeling.

From Figure 9a, it can be observed that there is again an excellent agreement for the  $CO_2^*/OH^*$  ratio except near the lean blow out limit of the combustor ( $\phi=0.66-0.69$ ). Both the model and experiment show a relatively small change in the ratio with fuel-air ratio over the range  $0.7 < \phi < 1$ . The results for the  $CH^*/OH^*$  ratio are shown in Figure 5b. The model reproduces the experimental data to within  $\sim 15\%$ , except near the lean blow out limit of the combustor.

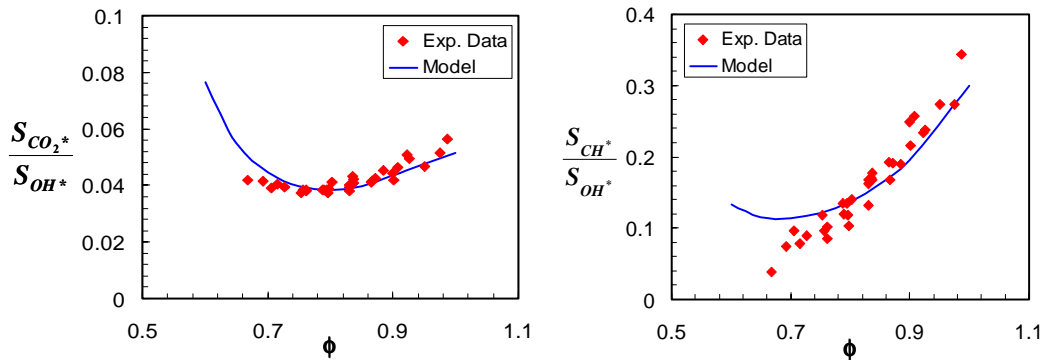


Figure 5. (a) Variation of  $CO_2^*$  to  $OH^*$  and (b) of  $CH^*$  to  $OH^*$  ratios in methane swirl combustor.

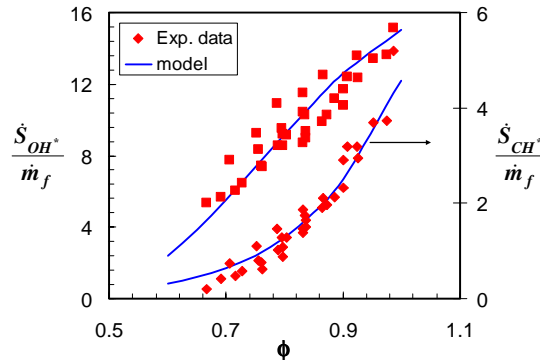


Figure 6. Normalized  $OH^*$  and  $CH^*$  chemiluminescence in methane swirl combustor.

As in the syngas tests, the normalized chemiluminescence signals were compared to the model predictions using equation (9). The results are displayed in Figure 6 for CH\* and OH\* emission. The CH\* model results lie within the experimental data spread as the OH\* model predictions. Near the lean blowout limit of the combustor, the OH\* data are above the model results, which the CH\* data are below. This explains the CH\*/OH\* drop off seen in Figure 5a. While not shown, the CO<sub>2</sub>\* predictions from the model are also within the experimental scatter over most of the  $\phi$  range. Therefore, we can conclude that the chemiluminescence models are reasonably accurate and can be used with appropriate chemical kinetic mechanisms to analyze the chemiluminescence signals from CO<sub>2</sub>\*, OH\* and CH\* in hydrocarbon flames.

## B. Chemiluminescence Interpretation

Two interesting applications of chemiluminescence for sensing and diagnostics that have been explored experimentally are heat release rate and flame zone equivalence ratio. For equivalence ratio sensing, ratios of chemiluminescence signals are employed. For example, it is typically reported that the CH\* to OH\* chemiluminescence ratio increases with  $\phi$ . Similarly, heat release rate is typically found by monitoring the chemiluminescence from one or more species and assuming that the chemiluminescence signal intensity is linearly proportional to heat release rate. Here we examine these approaches for syngas, methane and Jet-A systems. For the present studies, we examine chemiluminescence normalized by fuel flow rate. For complete combustion of fuel in lean flames this is a reasonable assumption. For rich flames, the heat release does not scale linearly with fuel flow rate because portions of the fuel are only partially oxidized. Still by comparing the model predictions normalized by fuel flow rate, we can get some idea of the chemiluminescence variation with heat release. Following equation (9), the fluorescence intensity  $I_c$  from the simulations are converted to a fuel flow rate normalized signal equation (10).

$$\frac{\dot{S}_c}{\dot{m}_f} \propto \frac{\dot{m}/\dot{m}_f}{\rho_u S_L} I_c \quad (10)$$

For sensing of heat release rate, one would ideally like the normalized fluorescence to be only weak functions of other flame conditions, such as equivalence ratio, reactant temperature and pressure.

### Syngas Fuels

From the simulations already shown in Figure 3, it is evident that the CO<sub>2</sub>\* to OH\* ratio (the only one available for H<sub>2</sub>/CO fuels) is nearly independent of  $\phi$  in the range of 0.75-1.0. However for leaner mixtures, the ratio is a strong function of  $\phi$ , rising quite steeply. This may be attributed to the lower flame temperatures, which affect the OH\* production more than CO<sub>2</sub>\*. So as a consequence, the OH\* intensity drops rapidly on the lean side compared to CO<sub>2</sub>\* emission. It is also interesting to note that for a given composition, dilution increases the ratios and preheating produces the opposite effect. Moreover, preheating and dilution do not qualitatively change the shape of the ratio plot. Finally, a change in composition of the fuel also leads to a change in the chemiluminescence ratio. Thus, it is seen that equivalence ratio monitoring using chemiluminescence ratios is not promising for fuels primarily composed of H<sub>2</sub> and CO, except under very lean conditions and for well known compositions and initial conditions.

Examining the simulated chemiluminescence signals normalized by fuel flow rate (Figure 4), it is seen that the normalized chemiluminescence is a function of fuel-air ratio. Over the range of  $\phi$  simulated (0.5-1.0), the normalized OH\* signal varies by roughly a factor of 7-10, while the CO<sub>2</sub>\* value changes by only about three times. Also even though the CO<sub>2</sub>\* production rate is proportional to the CO concentration, the CO<sub>2</sub>\* emission normalized by the mass flow rate of CO does not collapse the different fuel mixtures into a single curve. However for a fixed composition, neither dilution of the fuel (with CO<sub>2</sub> here) nor preheating (at least to ~500 K) causes the normalized emission to change significantly. For the OH\* data, the preheating and dilution now have a significant change on the normalized chemiluminescence, as does the fuel composition. At this juncture it should be pointed out that OH\* production in syngas systems depends on [H] and [O] radical concentrations in the flame. This can partly explain the apparent paradox of the lower H<sub>2</sub> containing syngas mixture producing higher OH\* signals on a normalized basis. In summary, neither OH\* nor CO<sub>2</sub>\* provide ideal conditions for heat release sensing under varying combustor conditions for syngas fuels. However, CO<sub>2</sub>\* does appear to be less sensitive to reactant temperature and dilution, and the variation with fuel-air ratio is less dramatic.

### Methane

For the methane validation tests above, the reactants were at room temperature. To examine preheating effects in more detail, simulations were carried out at a higher initial temperature (~500 K) and across a wider equivalence

ratio range (0.6-1.3). Results for two ratios ( $\text{CO}_2^*/\text{OH}^*$  and  $\text{CH}^*/\text{OH}^*$ ) are shown in Figure 7. Preheating the reactants by 200K produce little significant difference on the  $\text{CO}_2^*/\text{OH}^*$  ratio, except at very lean conditions. However, the variation of this ratio with  $\phi$  is not monotonic; there is both a local minimum ( $\phi \sim 0.75$ ) and local maximum ( $\phi \sim 1$ ). Thus, it would be difficult to use this ratio for  $\phi$  sensing. As shown in Figure 7b, on the other hand, the  $\text{CH}^*/\text{OH}^*$  ratio monotonically increases with equivalence ratio range and is only a weak function of reactant preheating; the maximum change is  $\sim 20\text{-}25\%$  over  $0.9 < \phi < 1.2$  for the 200 K variation, with less variation  $\sim 5\%$  at other  $\phi$ . Also, the ratio increases by  $15\times$  for  $\phi$  increasing from 0.6 to 1.3. Thus the model agrees with previous experimental studies showing that equivalence ratio can be sensed with a  $\text{CH}^*/\text{OH}^*$  ratio in methane flames.

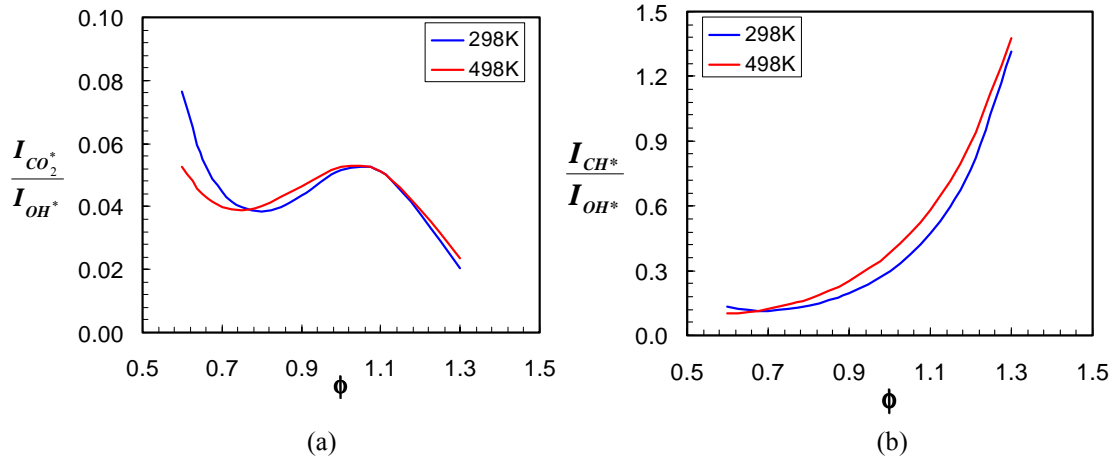


Figure 7. Simulation results for chemiluminescence ratios of (a)  $\text{CO}_2^*$  to  $\text{OH}^*$  and (b)  $\text{CH}^*$  to  $\text{OH}^*$  at two preheat temperatures for methane.

With regard to heat release sensing, the normalized chemiluminescence signals are shown in Figure 8. As seen in the syngas results, the normalized chemiluminescence is a function of equivalence ratio. In addition, Figure 8 shows that reactant preheating can also have a significant effect, with the ratios increasing with temperature. The  $\text{OH}^*$  and  $\text{CO}_2^*$  signals have similar non-monotonic dependence on equivalence ratio, while the  $\text{CH}^*$  signal increases monotonically with  $\phi$  over the range studied. Also, the relative change in the normalized chemiluminescence with  $\phi$  is greatest for  $\text{CH}^*$ , while the variation for  $\text{CO}_2^*$  is somewhat less than for  $\text{OH}^*$ . Thus while  $\text{CO}_2^*$  and to a lesser extent  $\text{OH}^*$  may be useful for sensing heat release rate variations for limited variations in  $\phi$  or reactant temperature conditions,  $\text{CH}^*$  is found to be much less suitable when changes in  $\phi$  occur.

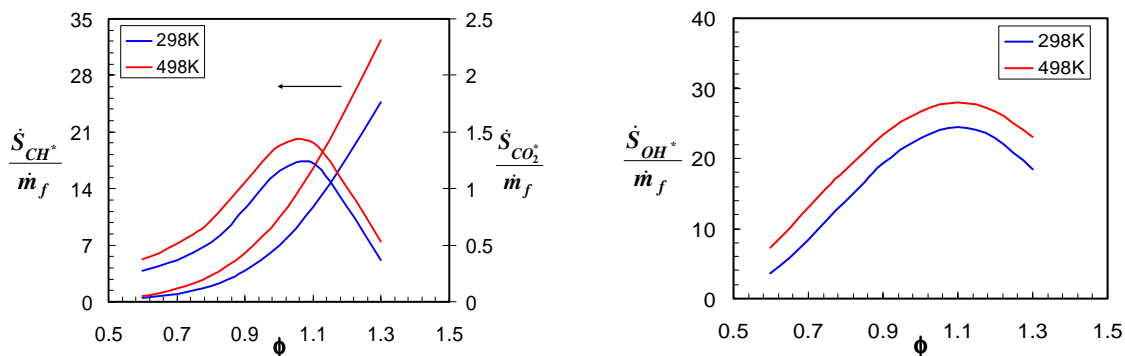


Figure 8. Normalized chemiluminescence signals simulated for (a)  $\text{CH}^*$  and  $\text{CO}_2^*$  and (b)  $\text{OH}^*$  for methane flames.

### Jet-A

While no validation of the chemiluminescence modeling is presented for Jet-A, the validation presented for the methane case gives some confidence in the application of the chemiluminescence model to a different hydrocarbon fuel. In fact, the greatest uncertainty in this case is likely to be the accuracy of the Jet-A mechanism employed. In

any case, the same methods were applied to Jet-A flames, i.e., assumptions of premixed conditions and 1-d flame modeling. Results are presented below for an equivalence ratio range of 0.55-1.35, typical of practical systems and for preheat temperatures of 450 and 650 K (350 and 710 °F).

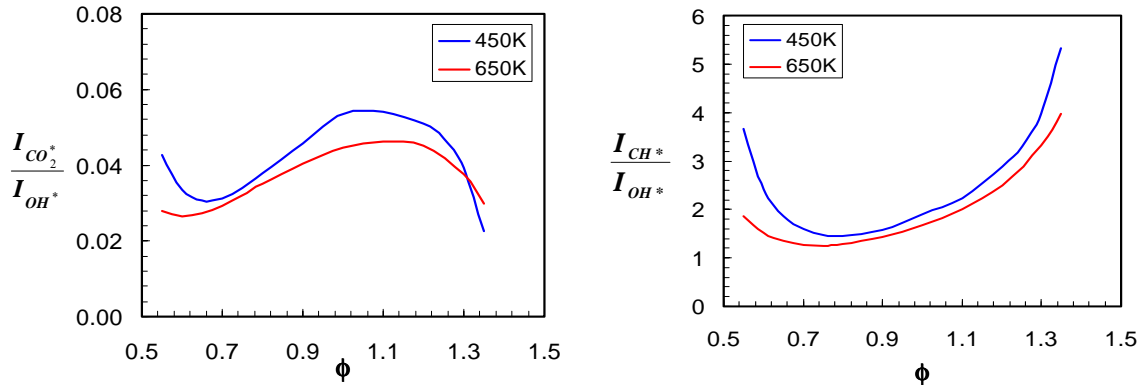


Figure 9. Modeling results for (a)  $CO_2^*$  and  $OH^*$  ratio, and (b)  $CH^*$  and  $OH^*$  ratio for Jet-A fuel.

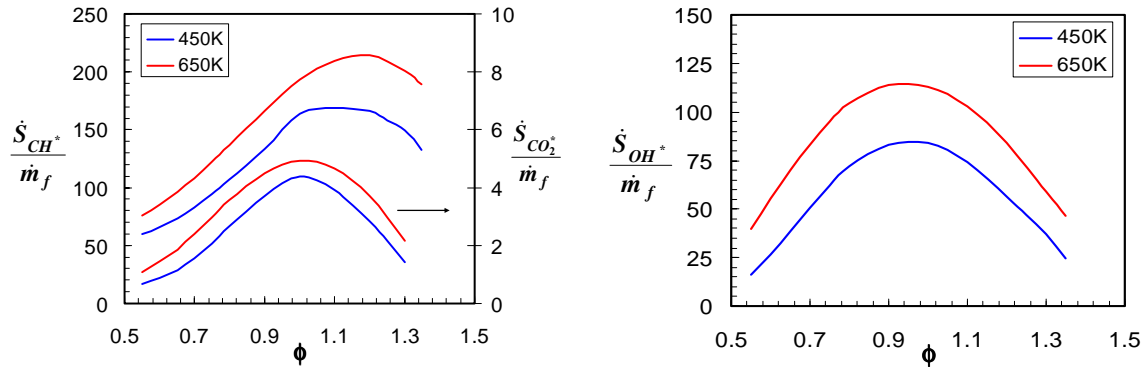


Figure 10. Modeling results for normalized (a)  $CH^*$ ,  $CO_2^*$ , and (b)  $OH^*$  chemiluminescence for Jet-A.

The chemiluminescence ratio results are shown in Figure 9. For Jet-A, neither ratio is monotonic with  $\phi$ . The  $CO_2^*/OH^*$  ratio is similar to the methane case, showing a local minimum and maximum. Unlike the methane results, the  $CH^*/OH^*$  is also non-monotonic, with a minimum near  $\phi=0.75$ . However, this ratio is less sensitive to reactant temperature. It can be seen in Figure 9b that a change in reactant temperature of 200K produces only a small difference in the  $I_{CH^*}/I_{OH^*}$  ratio, except at very lean and rich conditions. Thus these simulation results suggest that equivalence ratio may be possible with the  $CH^*/OH^*$  chemiluminescence ratio for either lean or rich conditions (away from the location of the minimum), but that reactant temperature may have to be taken into account. This is a potential drawback since flames with liquid fuels in practical combustors can involve some entrainment of products into the reactants, thereby changing the effective reactant temperature. It is also interesting to observe that for a given  $\phi$ , the ratios are generally higher than in the methane case (Figure 7). This is likely due to the fact that Jet-A is composed of higher order hydrocarbons that are more likely to produce  $C_2H$  as they react and therefore produce higher  $CH^*$  levels. The  $CO_2^*/OH^*$  ratio, on the other hand, is of nearly the same magnitude for Jet-A as for methane.

The normalized chemiluminescence signals are presented in Figure 10. As was found for methane, reactant temperature increase tends to raise the normalized chemiluminescence emission. However, when compared to methane, the relative change in the normalized  $CH^*$  and  $OH^*$  intensities with changes in  $\phi$  is reduced. In addition the normalized  $CH^*$  signal is no longer monotonic; this helps reduce the variation in the signal with  $\phi$ . As the normalized  $CO_2^*$  signal now varies more with  $\phi$ , it can only be used near  $\phi=1$  as a marker for heat release oscillations, assuming small changes in  $\phi$ . Whereas  $CH^*$  is now a better candidate in lean and rich conditions. Like  $CO_2^*$ ,  $OH^*$  is a good candidate for heat release sensing under varying conditions only around  $\phi=1$ . However, it is the

least preferable when it comes to the case of preheat fluctuations, as it is the most dependent on reactant temperature.

## VI. Conclusions

Recent advances in reaction rates for chemical formation of excited state species were assembled into a model for OH\*, CO<sub>2</sub>\* and CH\* chemiluminescence from hydrocarbon combustion. Chemiluminescence spectra were obtained from two premixed burners: a laminar jet flame for syngas mixtures and a swirl-stabilized methane combustor in order to validate the model. Both burners were operated over a range of equivalence ratios, and the syngas experiments also included variations in fuel composition, fuel dilution and reactant temperature. Simulations were performed with a standard 1-d, premixed flame code and a detailed flame chemistry mechanism (GRIMech 3.0). The results of these simulations were post-processed with the chemiluminescence model to predict flame chemiluminescence signals. Chemiluminescence ratios and chemiluminescence signals normalized with fuel mass flow rate were compared for the experiments and simulations. The agreement between the model and experimental results is excellent, with differences less than  $\pm 10\%$  for most cases. These differences are within the experimental accuracy and the probably within the ability of 1-d flame simulations to model more realistic flames. Thus the chemiluminescence model can be considered validated.

The model was then used to investigate the use of chemiluminescence for sensing applications in syngas, methane and Jet-A fuel systems. Specifically sensing equivalence ratio with ratios of chemiluminescence from two excited state species, and heat release rate sensing using absolute signals were considered. The latter was examined by considering the effect of fuel-air ratio, temperature and syngas fuel composition on the chemiluminescence signals normalized by fuel mass flow rate. For syngas fuels, the only available chemiluminescence ratio is  $S_{\text{CO}_2^*}/S_{\text{OH}^*}$ . This ratio is nearly independent of the equivalence ratio ( $\phi$ ) of the burning region for  $\phi > 0.7$ , but rises steeply as  $\phi$  is reduced below this value. Therefore,  $S_{\text{CO}_2^*}/S_{\text{OH}^*}$  can be used for fuel-air ratio sensing only for very lean mixtures. In addition, the chemiluminescence ratio depends on the H<sub>2</sub>/CO ratio in the fuel;  $S_{\text{CO}_2^*}/S_{\text{OH}^*}$  increases as the CO composition is raised. However, the ratio is only weakly dependent on reactant temperature and fuel dilution for the ranges studied. For methane,  $S_{\text{CH}^*}/S_{\text{OH}^*}$  is a good measure of equivalence ratio; it has a large and monotonic increase with equivalence ratio over the range studied and is only a weak function of reactant preheating. For Jet-A,  $S_{\text{CH}^*}/S_{\text{OH}^*}$  is still a good indicator of fuel-air ratio in the reaction region. However because it is no longer a monotonic function of  $\phi$ ,  $S_{\text{CH}^*}/S_{\text{OH}^*}$  can not be used if the  $\phi$  variation crosses the minimum in the chemiluminescence ratio around  $\phi = 0.75$ . Also, the reactant temperature may have to be taken into account.

For heat release rate sensing with simultaneous changes in either  $\phi$  or reactant temperature, as might be expected in combustors operating with stratified mixtures or in the presence of combustion oscillations, none of the chemiluminescence species studied are ideal. All three, OH\*, CO<sub>2</sub>\* and CH\*, produce chemiluminescence signals that vary with equivalence ratio even for fixed heat release. For a fixed syngas fuel composition, CO<sub>2</sub>\* chemiluminescence is less sensitive to reactant temperature, fuel dilution and fuel-air ratio variations than OH\*. For example for an average  $\phi = 0.8$  with a variation of  $\pm 0.1$ , the CO<sub>2</sub>\* chemiluminescence signal varies by about  $\pm 20\%$  for a fixed heat release rate. For methane combustion, the chemiluminescence signals show an increased dependence on reactant temperature. CO<sub>2</sub>\* or possibly OH\* chemiluminescence can be useful for sensing heat release rate variations for limited variations in  $\phi$  or reactant temperature conditions. CH\* is a poorer choice in the presence of fuel-air ratio changes. For Jet-A combustion, CO<sub>2</sub>\* and OH\* are good candidates for heat release sensing near stoichiometric conditions, as both exhibit reduced dependence on  $\phi$  in that region. CO<sub>2</sub>\* sensing is preferable if reactant temperature is also expected to vary. CH\* is a more suitable candidate in lean conditions as it exhibits a lower  $\phi$  dependence there than the other candidates.

## Acknowledgments

This research was supported by NASA through the University Research, Engineering, and Technology Institute for Aeropropulsion and Power, under Grant/Cooperative Agreement Number NCC3-982.

## References

- <sup>1</sup> Gaydon, A. G., Wolfhard, H. G. *Flames: Their Structure, Radiation, and Temperature*. Fourth edition, Chapman and Hall, 1978.
- <sup>2</sup> Kojima, J., Ikeda, Y., Nakajima, T., “Spatially resolved measurement of OH\*, CH\* and C<sub>2</sub>\* chemiluminescence in the reaction zone of laminar methane/air premixed flames”, Twenty eighth Symposium (International) on Combustion, 2000, pp. 1757-1764.
- <sup>3</sup> Docquier, N., Lacas, F., Candel, S., “Closed-loop equivalence ratio control of premixed combustion using spectrally resolved chemiluminescence measurements”, Twenty ninth symposium (International) on Combustion, 2002, pp 139-145.
- <sup>4</sup> Muruganandam, T. M., Kim, B. H., Morrell, M. R., Nori, V., Patel, M., Romig, B. W., Seitzman, J. M., “Optical equivalence ratio sensors for gas turbine combustors,” Thirtieth symposium (International) on Combustion, 2005, pp. 1601-1609, Part 1.
- <sup>5</sup> Yamazaki, M., Ohya, M., Tsuchiya, K. *Int. Chem. Eng.* **30** (1992), pp. 160–168.
- <sup>6</sup> Stojkovic, B. D., Fansler, T. D., Drake, M. C., and Sick, V., “High-speed imaging of OH\* and soot temperature and concentration in a stratified-charge direct-injection gasoline engine,” ,” Thirtieth symposium (International) on Combustion, 2005, 2657-2665 Part 2, 2005
- <sup>7</sup> Lee, J. G., Kim, K., Santavicca, D. A., “Measurement of Equivalence Ratio Fluctuation and Its Effect in Heat Release During Unstable Combustion,” *Proceedings of the Combustion Institute*, Vol. 28, 2000, pp. 415–421.
- <sup>8</sup> Bellows, B. D., Zhang, Q., Neumeier, Y., Lieuwen, T., and Zinn, B. T., “Forced Response Studies of a Premixed Flame to Flow Disturbances in a Gas Turbine Combustor,” AIAA Paper 2005-1164, Jan. 2005.
- <sup>9</sup> Najm, H. N., Paul, P. H., Mueller, C. J., Wyckoff, P. S., *Combustion and Flame* 113 (3) (1998) 312-332.
- <sup>10</sup> Smith, G. P., Luque, J., Park, C., Jeffries, J. B., Crosley, D. R., “Low pressure flame determinations of rate constants for OH(A) and CH(A) chemiluminescence,” *Combustion and Flame*, Vol. 131 (1-2), pp. 59-69, 2002.
- <sup>11</sup> Kojima, J., Ikeda, Y., Nakajima, T., “Basic Aspects of OH(A), CH(A), and C<sub>2</sub>(d) Chemiluminescence in the Reaction Zone of Laminar Methane-Air Premixed Flames,” *Combustion and Flame*, Vol. 140, 2005, pp. 34-45.
- <sup>12</sup> Haber, L. C., Vandsburger, U., Saunders, W. R., Khanna, V. K., “An Examination of the Relationship between Chemiluminescent Light Emissions and Heat Release Rate under Non-Adiabatic Conditions,” *Proceedings of International Gas Turbine Institute*, 2000.
- <sup>13</sup> Samaniego, J. M., Egolfopoulos, F. N., Bowman, C. T., “CO<sub>2</sub>\* Chemiluminescence in Premixed Flames,” *Combustion Science and Technology*, Vol. 109, pp. 183-203, 1995.
- <sup>14</sup> Moliere, M., “Benefitting from the Wide Fuel Capability of Gas Turbines: A Review of Application Opportunities,” ASME paper GT-2002-30017, 2002.
- <sup>15</sup> Carrington, T., “Electronic Quenching of OH (<sup>2</sup>Σ<sup>+</sup>) in Flames and Its Significance in the Interpretation of Rotational Relaxation,” *Journal of Chemical Physics*, Vol. 30, No. 4, 1959, pp. 1087-1095.
- <sup>16</sup> Kaskan, W. E., “Abnormal Excitation of OH in H<sub>2</sub>/O<sub>2</sub>/N<sub>2</sub> Flames,” *Journal of Chemical Physics*, Vol. 31, No. 4, 1959, pp. 944-956.
- <sup>17</sup> Belles, F. E. and Lauver, M. R., “Origin of OH Chemiluminescence during the Induction Period of the H<sub>2</sub>-O<sub>2</sub> Reaction behind Shock Waves,” *Journal of Chemical Physics*, Vol. 40, No. 2, 1964, pp.415-417.
- <sup>18</sup> Hidaka, Y., Takahashi, S., Kawano, H., Suga, M., and Gardiner, W. C. Jr., “Shock-Tube Measurement of the Rate Constant for Excited OH (A<sup>2</sup>Σ<sup>+</sup>) Formation in the Hydrogen-Oxygen Reaction,” *Journal of Physical Chemistry*, Vol. 86, No. 8, 1982, pp. 1429-1433.
- <sup>19</sup> Petersen E. L. and Kalitan, D. M., “Calibration and Chemical Kinetics Modeling of an OH Chemiluminescence Diagnostic,” AIAA 2003-4493, 39th AIAA/ASME/SAE/ASEE Joint Propulsion Conference and Exhibit, 20-23 July 2003, Huntsville, Alabama
- <sup>20</sup> Carl, S. A., Poppel, V. M., and Peeters, J., “Identification of the CH + O<sub>2</sub> → OH (A) + CO Reaction as the Source of OH(A-X) Chemiluminescence in C<sub>2</sub>H<sub>2</sub>/O/H/O<sub>2</sub> Atomic Flames and Determination of its Absolute Rate Constant over the Range T = 296 to 511 K”, *Journal of Physical Chemistry A*, 2003, Vol. 107, pp. 11001-11007.

- <sup>21</sup> Tamura, M.; Berg, P. A.; Harrington, J. E.; Luque, J.; Jeffries, J. B.; Smith, G. P.; Crosley, D. R. *Combust Flame* 1998, **144**, 502-514.
- <sup>22</sup> Hall, J. M., Petersen, E. L., "An optimized kinetics model for OH chemiluminescence at high temperatures and atmospheric pressures," *International Journal of Chemical Kinetics*, 38 (12), pp. 714-724, 2006
- <sup>23</sup> Privilov, A. M., and Smirnova, L. G., "Temperature-Dependence of the Spectral Distribution of the Rate-Constant of Chemiluminescence in the Reaction  $O(3P)+CO\rightarrow CO_2+h\nu$ ," *Kinetics and Catalysis* 22 (4): 832-838, 1981.
- <sup>24</sup> Baulch, D. L., Drysdale, D. D., Duxbury, J. and Grant, S. J. *Evaluated Kinetic Data for High Temperature Reactions* Vol. 3, Butterworths, London, 1976.
- <sup>25</sup> Slack, M., Grillo, A., "High-Temperature Rate Coefficient Measurements of  $CO + O$  Chemi-luminescence," *Combustion and Flame* 59 (2): 189-196 1985.
- <sup>26</sup> Gaydon, A. G. *The Spectroscopy of Flames*, 2nd ed, Chapman and Hall: London, 1974.
- <sup>27</sup> Brenig, H. H., Ph.D. Thesis, Wuppertal, 1981.
- <sup>28</sup> Grebe, J.; Homann, K. H. *Ber. Bunsen-Ges. Phys. Chem.*, 86, 587, 1982.
- <sup>29</sup> Glass, G. P.; Kistiakowsky, G. B.; Michael, J. V.; Niki, H. *Symp.(Int.) Combust. [Proc.]*, 10, 513, 1965.
- <sup>30</sup> Renlund, A. M.; Shokoohi, F.; Reisler, H.; Wittig, C. *J. Phys. Chem.*, 86, 4165, 1982
- <sup>31</sup> Devriendt, K.; Peeters, J. *J. Phys. Chem. A*, 101, 2546, 1997.
- <sup>32</sup> Elsamra, R. M. I., Vranckx, S., Carl, S. A. *J. Phys. Chem. A*, 109, 10287, 2005.
- <sup>33</sup> CHEMKIN<sup>TM</sup>, [www.ReactionDesign.com](http://www.ReactionDesign.com)
- <sup>34</sup> Smith, G. P., Golden, D. M., Frenklach, M., Moriarty, N. W., Eiteneer, B., Goldenberg, M., C. T. Bowman, C. T., Hanson, R. K., Song, S., Gardiner, W. C. Jr., Lissianski, V. V., Qin, X., [http://www.me.berkeley.edu/gri\\_mech/mech/](http://www.me.berkeley.edu/gri_mech/mech/)
- <sup>35</sup> Elliott, L., Ingham, D.B., Kyne, A.G., Mera, N.S., Pourkashanian, M. and Wilson, C.W., "A novel approach to the reduction of an aviation fuel/air reaction mechanism using a genetic algorithm", *Proceedings of ASME Turbo Expo 2004: Land, sea and air*, Vienna, Austria, GT-2004-53053.